

# Design of a Piezoelectric Meso-scale Mobile Robot: A Compliant Amplification Approach

V. K. Varma<sup>†</sup> and W. E. Dixon<sup>‡</sup>

<sup>†</sup>Nuclear Science & Technology Division - Remote Systems, <sup>‡</sup>Engineering Science & Technology Division - Robotics,  
Oak Ridge National Laboratory, Oak Ridge, TN, 37831-6305, email: varmavk, dixonwe@ornl.gov

**Abstract:** In this paper, the development of a novel piezoelectric-based locomotion design for a meso-scale mobile robot is described. The design exploits a compliant mechanical structure that enables piezoelectric forces to be amplified and transmitted to “legs” that propel the robot through a lift and pull scheme. The lift and pull design contrasts with typical slip/stick approaches that assume the inertia effects of the robot will allow the robot to slip on a smooth surface. By eliminating the slipping assumption, the potential surfaces that the proposed robot can traverse is significantly extended. Discussions are provided regarding the proposed locomotion method, kinematic modeling and system constraints, mechanical optimization, and control of the meso-scale robot.

## I. INTRODUCTION

A significant interest in miniaturized robotic systems has recently been spawned by various applications including: inspection, miniature manipulation, exploration, and search and rescue. Since many of the concepts and tools that have been developed for traditional robotic systems cannot typically be scaled down to the meso, micro, or nanometer size<sup>1</sup> of recently conceptualized miniature robots, researchers have been actively investigating new methods for robotic manipulation and locomotion. Although a consensus seems to exist among researchers regarding miniaturized manipulation using a tweezer like mechanism or a pipette (e.g., see [15], [18], [21] and the references within), a wide variety of mechanisms have been investigated for miniaturized robotic locomotion. For example, in [19], Teshigahara et al. utilized a traditional step-motor design that was reduced to the micro-scale to actuate a meso-scale car ( $7 \times 2.8 \times 3$  mm). However, as reported in [19], the micro step-motor based locomotion technique had several severe drawbacks: (i) due to the use of joints, the friction caused excessive wear on the micromachined parts, (ii) the use of lubricants were shown to act as an adhesive rather than a lubricant, further highlighting the problem of friction and wear, and (iii) for rough surfaces (e.g., 200  $\mu$ m sand paper), the robot vibrated in place rather than traversing a path. In [7] and [8], Ioi developed a locomotion technique for a meso-scale robot ( $28 \times 10 \times 4.5$  mm) that utilizes two motors to create centrifugal forces on the rigid body, resulting in motion of the robot through brush fibers. One of the main drawbacks of the locomotion technique developed in [7] and [8] is that the brush fibers are not directly actuated; hence, (i) significant power is lost in the passive transmission of the centrifugal forces to the brush fibers, (ii) the brush fibers have a propensity to slip

(in the experimental results presented in [8], red chalk-powder was placed on glass to reduce the slipping effects), and (iii) the velocity of the robotic platform is significantly influenced by the surface. In [10], Laurent and Piat developed a meso-scale ( $50 \times 10 \times 10$  mm) fish-like robot that exploits an ionic polymer metal composite to produce an undulatory motion of the fins (with mean speeds of 1.8 mm/sec).

In addition to the various locomotion techniques described above, several researchers have investigated the use of piezo-based locomotion techniques. For example, in [1] Aoyama and Fuchiwaki utilized a combination of piezoceramic bimorph and electromagnetic actuators to develop meso-scale mobile robots ( $20 \times 20 \times 18$  mm) that are able to move objects in a scanning electron microscope (SEM) vacuum chamber. With an approximate speed of 1.16 mm/sec, the meso-scale robots developed in [1] achieved locomotion through an inchworm-like motion: the use of electromagnets also allows the meso-scale robots to climb the walls of the steel SEM chamber. In [6], [15], [16] piezoceramic bimorph actuators were utilized to enable a slip/stick locomotion technique [2] (similar to the inchworm-like motion of [1]) to enable the MINIMAN series of robots to perform mobile manipulation tasks. The slip/stick locomotion technique utilized in [6], [15], [16] is based on the principle that when voltage is applied to the piezoceramic bimorph leg, the leg bends; however, due to inertia forces, the leg slips on the surface resulting in no forward/reverse motion by the robot. When the voltage is removed, the legs straighten, resulting in a pulling/pushing motion of the robot platform. As reported in [6], when a voltage of  $\pm 150$  V with a frequency of 5 kHz was applied to the piezoceramic bimorph legs of MINIMAN-I, the robot achieved a maximum velocity of 3 cm/sec on a glass surface. In [11]-[14], Martel et al. utilize a similar locomotion technique as described in [6] for the meso-scale robot (32 mm in diameter) dubbed NanoWalker due to the nanometer step size capabilities. The NanoWalker has 3 piezoceramic legs that are responsible for locomotion (at 100 V, speeds of less than 15 mm/sec were reported) and for power (i.e., the NanoWalker is constrained to move along a specialized surface that supplies power to the robot through its legs). The NanoWalker also requires sophisticated walking algorithms to be employed due to the unstable, three legged design.

In addition to the slip/stick piezo-based locomotion techniques, several researchers have also investigated other piezo-based locomotion methods that use the piezo element as an input force to a mechanical amplification mechanism. Specifically, in [20], Yan et al. utilized various piezo-based unimorph actuators to produce forces that were amplified through a four-bar linkage to rotate the wing of a meso-scale (25 mm wingspan) aerial vehicle. The kinematic analysis given in [20] indicated that the four-bar mechanism could amplify an input of 0.1 mm to achieve  $180^\circ$  of wing rotation. In [17], Sitti developed the kinematic and dynamic models for the aerial vehicle given in [20] and describes issues related to the mechanical optimization. In [3] and [4], Cox et al. developed piezo-based unimorph

This research was supported in part by the Eugene P. Wigner Fellowship Program of the Oak Ridge National Laboratory (ORNL), managed by UT-Battelle, LLC, for the U.S. Department of Energy (DOE) under contract DE-AC05-00OR22725 and in part by the U.S. DOE Environmental Management Sciences Program (EMSP) projects ID No. 82797 and ID No. 82794 at ORNL.

<sup>1</sup>Due to the vast differences in the technologies that can be applied, which directly depend on the scale of the robot and the application, in this paper we have elected not to categorize all of the miniaturized systems under the canopy of microelectromechanical systems (MEMS). Rather, we utilize the term meso-scale, micro-scale, and nano-scale to describe systems that range from 1-100 mm, 1-100  $\mu$ m, and 1-100 nm, respectively.

and bimorph flapping mechanisms for a meso-scale aerial vehicle. In contrast to the pin-joint dependent four-bar mechanism utilized in [20], amplification of the piezo-input in [3] and [4] was achieved through the use of compliant structures. In [9], Kota et al. presented a generalized methodology for developing compliant mechanisms that provides a basis for topology generation and size and shape optimization for general MEMS. To illustrate the compliant structure amplification technique, [9] developed a series of four-bar linkages that provided for an amplification factor of 20.

In this paper, we describe the initial development of a Piezo-electric actuated meso-scale ( $35 \times 35 \times 6$  mm) Mobile Robot (PMR) that employs a new piezo-based locomotion technique that results from piezoelectric forces that are amplified through a compliant lever-based flexure. Specifically, the output from a lead zirconate titanate (PZT) piezoelectric element is connected to a compliant titanium linkage that results in an amplification of the piezo displacement. The final section of the compliant titanium linkage is connected to a “leg” element, resulting in a lifting and pulling force that propels the robot. In comparison with [6], and [11]-[14], the advantages of the proposed locomotion method are that: (i) the approach does not require the assumption that the actuated leg slips on the surface, (ii) complex “walking” algorithms are not required, and (iii) significantly improved speeds are facilitated (e.g., 65 cm/sec). In comparison with the four-bar linkage mechanism given in [17] and [20] or the motor driven mechanisms given in [7], [8], [19], the proposed compliant amplification structure does not utilize joints, and hence, as described in [9], problems associated with wear, backlash, noise, and the need for lubrication, are eliminated.

This paper is organized as follows. In Section II, we describe the locomotion principle (motivated by the advantages and disadvantages of related work in literature) that lead to the proposed PMR design. In Section III, the kinematic model of the PMR is developed along with several constraints. In Section IV, a discussion is provided regarding the optimization of the mechanical design. In Section V, a discussion regarding the control of the PMR is provided. In Section VI, concluding remarks are presented.

## II. LOCOMOTION PRINCIPLE

From the review of literature given previously, it seems that most of the methods developed to actuate meso-scale robots either utilize scaled-down motor assemblies or utilize some form of piezo-based actuation. When compared to scaled down motor-based approaches, potential advantages of piezo-based actuation methods include: (i) significantly increased power/volume ratio, (ii) reduced cost, and (iii) improved accuracy. Typical piezo-based actuator designs for mobile ground robots target applications where small step size is required, speed is not a main motivating factor, and the surface is highly controlled (flat and slippery). For these applications, the piezo-based actuator is typically placed directly in contact with the surface and a slip/stick locomotion mechanism is utilized (e.g., [1], [2], [6], [11]-[14], [15], [16]). As illustrated in Figure 1, the slip/stick locomotion mechanism is based on the assumption that the piezo-based actuator slips on the contact surface. Specifically, as illustrated in Figure 1, when a voltage is applied to the piezo-based actuator, it bends and is assumed to slip on the contact surface. Since the actuator slips on the contact surface, no forward motion is produced. When the voltage is removed from the actuator, it straightens and is assumed to stick. Since the actuator is assumed to stick during this phase, a resulting force is produced that propels the robot forward. Clearly, this type

of locomotion method is constrained by the type of surface that can be navigated. For example, Fahlbusch et al. [6] states that a smooth, flat glass surface was utilized to demonstrate the slip/stick approach utilized by the MINIMAN-I robot and in [11] a specialized surface was developed to both power the robot and to facilitate the slip/stick locomotion principle.

Provided the contact surface can be controlled and that the speed of the robot is not a motivating factor of the design, robots that use the slip/stick locomotion principle may be applicable. However, some applications do not meet these stringent conditions, providing motivation for additional locomotion principles. A characteristic of piezo-based actuators that must be addressed by new locomotion principles is the limited displacement that is produced by the actuator. For example, current piezoelectric devices typically produce strain forces on the order of 0.1% (e.g., a piezoelectric element with a height 5mm produces 0.005mm of displacement). The approach taken by researchers investigating the design of meso-scale aerial vehicles to overcome the limited displacement of piezo-based actuators is to amplify the displacement via a jointed four-bar linkage. One drawback of the jointed four-bar linkages is that joints require clearance to allow for the movement of the mating parts and developing joint clearance at the required scale is a significant issue due to friction effects (this phenomenon is one of the limiting factors of motor-based designs at the meso to nano-scale). As a means to alleviate the need for joints, recent research in [3], [4], and [9] has highlighted the use of compliant mechanical elements.

Inspired by the displacement amplification principles developed for meso-scale aerial vehicles and by the results described in [3], [4], and [9], a piezo-based locomotion technique is proposed that is based on displacement amplification through compliant lever-based flexural elements that actuate a rigid leg. The lever-based flexural elements allow for specific points in the structure to deflect, thus providing a desired amplification of the motion at the leg. A potential drawback of displacement amplification is that the force producing the displacement is reduced by an equivalent amount. However, since meso-scale robots are typically low weight and since piezo-materials can exert extremely high forces, it seems that acceptable displacement/force ratios can be designed.

The particular PMR design that we developed using this locomotion principle is illustrated in Figure 2. As illustrated in Figure 2, the stroke of two piezoelectric elements are amplified by a series of compliant lever-based structures that have legs affixed to the final lever bars. As illustrated in Figure 1, the movement of the legs results in a lifting motion when voltage is applied to the piezoelectric element and when voltage is removed from the piezoelectric element, the leg pulls the PMR forward. In addition, two passive wheels are incorporated in the design to serve the dual purpose of supporting the vehicle and for providing odometry information about the vehicle’s location. In comparison with the typical slip/stick approach, the proposed approach does not require the assumption that the leg will slip on the surface; hence, enabling the robot to traverse significantly expanded terrain. Moreover, due to the amplified displacement of the piezoelectric element, the resulting leg velocity is significantly greater than typical velocities obtained using the slip/stick approach (e.g., speeds of greater than 65 cm/sec are easily obtained).

## III. MODEL DEVELOPMENT

### A. Linkage Kinematic Model

The forward kinematics for the linkage system given in Figures 3 and 4 relate the task-space coordinates, denoted by

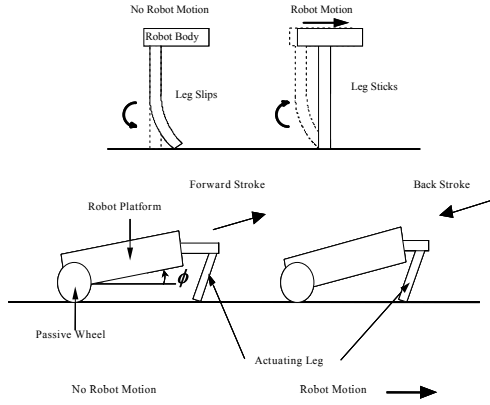


Fig. 1. Comparison of the slip/stick approach to the proposed locomotion approach

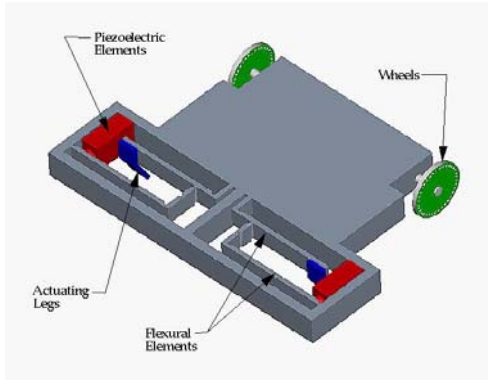


Fig. 2. Mobility platform using two piezoelectric actuators

$\xi(t) = [x_G \ y_G \ \theta_G]^T \in \mathbb{R}^3$ , of the Cartesian position and orientation of the coordinate frame attached to point  $G$  to the coordinate frame attached to point  $A$  as a function of the joint-space<sup>2</sup> variables denoted by  $q_L(t) = [\theta_1 \ \theta_2 \ \theta_4 \ \theta_5]^T \in \mathbb{R}^4$ . Specifically, the forward kinematics are given as follows

$$\xi = h(q_L) = \begin{bmatrix} L_2 c_1 + L_3 (s_{1+2} - s_{5-4}) + (L_5 - L_4) c_5 \\ L_2 s_1 - L_3 (c_{1+2} + c_{5-4}) + (L_5 - L_4) s_5 \\ \theta_5 \end{bmatrix} \quad (1)$$

where the notation  $c_{\zeta 1}$  and  $s_{\zeta 1}$  denote the  $\cos \theta_{\zeta 1}$  and  $\sin \theta_{\zeta 1}$ , respectively, the subscript “1 + 2” represents the sum  $\theta_1 + \theta_2$  and the subscript “1 - 2” represents the difference  $\theta_1 - \theta_2$ . A linkage Jacobian-like expression, denoted by  $J(q_L) \in \mathbb{R}^{3 \times 4}$ , can be obtained as follows

$$\dot{\xi} = \frac{\partial h(q_L)}{\partial q_L} \dot{q}_L = J \dot{q}_L \quad (2)$$

where  $J(q_L)$  is defined as follows

$$J = \begin{bmatrix} -L_2 s_1 + L_3 c_{1+2} & L_3 c_{1+2} & L_3 c_{5-4} \\ L_2 c_1 + L_3 s_{1+2} & L_3 s_{1+2} & -L_3 s_{5-4} \\ 0 & 0 & 0 \\ -L_3 c_{5-4} - (L_5 - L_4) s_5 & & \\ L_3 s_{5-4} + (L_5 - L_4) c_5 & & \\ & & 1 \end{bmatrix}. \quad (3)$$

<sup>2</sup>In subsequent development, we utilize the word joint to describe the compliant flexure point, however, this notation should not be confused with traditional joints.

Given (2), the time derivative of the joint-space variables is related to the time derivative of the position and orientation of the actuated leg with respect to a body fixed reference frame. In the next section, we will relate the time derivative of the position and orientation of the actuated leg to the linear and angular velocity of the vehicle body with respect to an inertial reference frame.

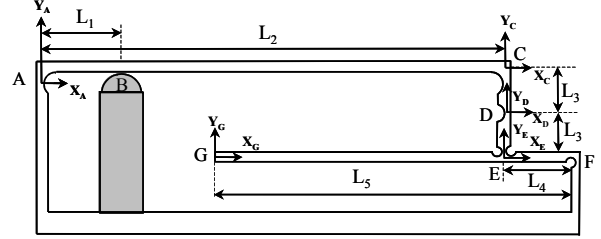


Fig. 3. Linkage diagram for the right-half of the PMR

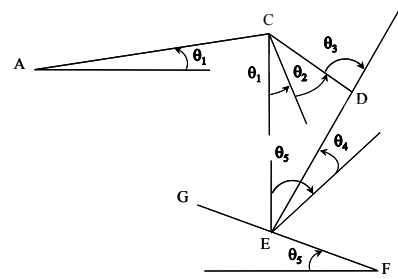


Fig. 4. Angle diagram for PMR linkages

*Remark 1:* The forward kinematics given in (1) were developed for half of the linkages contained in the overall PMR design. Given the symmetry of the PMR, the expression for  $\xi(t)$  can be written in terms of the left and right actuators (i.e.,  $\xi_L(t) = [x_{GL} \ y_{GL} \ \theta_{GL}]^T$  and  $\xi_R(t) = [x_{GR} \ y_{GR} \ \theta_{GR}]^T$ ).

*Remark 2:* The expression given in (1) and (2) provides a relationship between the task-space position and orientation of an actuated leg and the joint-space variables. The expression given in (3) is denoted as a Jacobian-like term rather than the Jacobian, to distinguish the fact that the joint-space variables are not control variables. Through various constraint equations developed in a subsequent section, the PMR is reduced to a one degree-of-freedom system. Based on the fact that  $\theta_3(t)$  is constrained by  $\theta_1(t)$ ,  $\theta_2(t)$ ,  $\theta_4(t)$ , and  $\theta_5(t)$ , it is not included in the Jacobian-like expression given in (3). That is, the task-space motion of the leg is dependant on  $\theta_3(t)$  only through a subsequently developed system constraint that is a function of the other joint angles.

### B. Vehicle Kinematic Model

The kinematic model that describes the task-space motion of the vehicle with respect to an inertial reference frame is given as follows [5]

$$\dot{q}_v = S(q_v)v \quad (4)$$

where the vehicle position and velocity, denoted by  $q_v(t)$ ,  $\dot{q}_v(t) \in \mathbb{R}^3$ , are defined as follows

$$q_v = [x_c \ y_c \ \theta_c]^T \quad \dot{q}_v = [\dot{x}_c \ \dot{y}_c \ \dot{\theta}_c]^T. \quad (5)$$

For the kinematic model given in (4) and (5),  $x_c(t)$  and  $y_c(t)$  denote the Cartesian position of the center of mass (COM) of the PMR along the X and Y-coordinate axis of the reference inertial frame (see Figure 5),  $\theta_c(t) \in R^1$  represents the orientation of the PMR with respect to the reference inertial frame (see Figure 5),  $\dot{x}_c(t)$ ,  $\dot{y}_c(t)$  denote the Cartesian components of the linear velocity of the COM,  $\dot{\theta}_c(t) \in R^1$  denotes the angular velocity of the COM, the matrix  $S(q_v) \in R^{3 \times 2}$  is defined as follows

$$S(q_v) = \begin{bmatrix} \cos \theta_c & 0 \\ \sin \theta_c & 0 \\ 0 & 1 \end{bmatrix}, \quad (6)$$

and  $v(t) = [v_1 \ v_2] \in R^2$  denotes the linear and angular velocity of the PMR. To relate the linear and angular velocity of the PMR to the linear velocity of the actuated legs, the following relationship is formulated

$$v = \begin{bmatrix} \frac{1}{D} & \frac{1}{D} \\ \frac{1}{D} & -\frac{1}{D} \end{bmatrix} \begin{bmatrix} \dot{y}_{GL} \cos \phi \\ \dot{y}_{GR} \cos \phi \end{bmatrix} \quad (7)$$

where  $\dot{y}_{GL}(t)$ ,  $\dot{y}_{GR}(t)$  denote the time derivative of  $y_{GL}(t)$ ,  $y_{GR}(t)$  described in Remark 1,  $\phi \in R^1$  denotes the angle of the PMR body with respect to the plane of the inertial reference frame (see Figure 1), and  $D \in R^1$  represents the distance between the passive wheels along the wheel axis (see Figure 5). Hence, based on (4) and (7), the time derivative of the position of the actuated leg is related to the time derivative of the position and velocity of the vehicle body in the inertial reference frame coordinates.

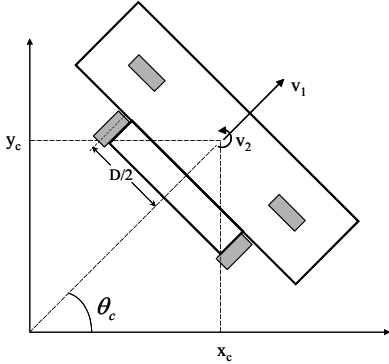


Fig. 5. Relationship between the PMR and the inertial reference frame

### C. Constraint Equations

Based on the construction of the linkages, several constraints are imposed on the PMR. Specifically, from the geometric relationships obtained from Figures 3 and 4, the following constraints can be formulated

$$L_2 c_1 + L_3 (s_{1+2} - s_{5-4}) = L_2 + L_4 (1 - c_5) \quad (8)$$

$$L_2 s_1 - L_3 (c_{1+2} + c_{5-4}) = -2L_3 + L_4 s_5 \quad (9)$$

$$y_B = L_1 \tan \theta_1 \quad (10)$$

$$\theta_3 = \theta_1 + \theta_2 + \theta_5 - \theta_4 \quad (11)$$

where  $y_B(t) \in R^1$  represents the displacement of the piezoelectric structure at point B along the Y-coordinate axis of the coordinate frame attached to point A. In addition to the kinematic constraints, several dynamic constraints are also imposed on the system. For example, by performing a moment balance

at points A, C, E, and F (see Figures 3 and 4), the following constraints are obtained

$$F_{yC} L_2 = F_{yB} L_1 - k_1 \theta_1 + k_2 \theta_2 \quad (12)$$

$$F_{xD} L_3 = k_2 \theta_2 + k_3 \theta_3 \quad (13)$$

$$L_3 (F_{yD} s_3 - F_{xD} c_3) = k_3 \theta_3 - k_4 \theta_4 \quad (14)$$

$$F_{yE} L_4 = F_{yG} L_5 + k_4 \theta_4 + k_5 \theta_5. \quad (15)$$

In the constraint equations given in (12-15),  $F_{yB}(t) \in R^1$  represents the piezoelectric force at point B that is assumed<sup>3</sup> to be defined as follows

$$F_{yB} = \frac{F_{\max} (y_{\max} - y_B)}{y_{\max}} \quad (16)$$

which results from displacing the piezoelectric element where  $F_{\max}, y_{\max} \in R^1$  represent the known, maximum force and displacement of the piezoelectric element for a given voltage input, and  $F_{yC}(t)$ ,  $F_{yE}(t)$ ,  $F_{yG}(t) \in R^1$  represent the forces applied along the Y-coordinate axis of the coordinate frames attached at points C, E, and G, respectively,  $F_{xC}(t)$ ,  $F_{xD}(t)$ ,  $F_{xE}(t) \in R^1$  represent the forces applied along the X-coordinate axis of the coordinate frames at points C, D, and E, respectively, and  $k_i \in R^1$  represent the spring constants defined as follows

$$k_i = \frac{E b h_i^3}{12 L} \quad \forall i = 1, 2, \dots, 5 \quad (17)$$

at the compliant joints  $\theta_i \forall i = 1, 2, \dots, 5$ , respectively. In (17),  $E$  denotes Young's modulus, and  $b, h_i, L \in R^1$  represent the depth, width, and length of the  $i$ -th compliant joint (see Figure 6). In addition to the moment balance constraints, the following force balance constraints can be formulated (see Figures 3 and 4)

$$F_{xD} = -F_{xC} c_2 - F_{yC} s_2 \quad (18)$$

$$F_{yD} = F_{xC} s_2 - F_{yC} c_2 \quad (19)$$

$$F_{xD} c_3 - F_{yD} s_3 + F_{xE} c_4 + F_{yE} s_4 = 0 \quad (20)$$

$$F_{xD} s_3 + F_{yD} c_3 - F_{xE} s_4 + F_{yE} c_4 = 0. \quad (21)$$

As described in Section II, the motion of the PMR can be de-

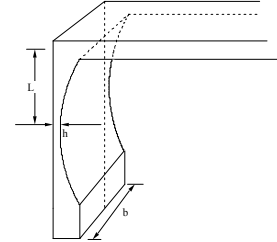


Fig. 6. Compliant joint cross-section

scribed by a lifting phase and a pulling phase. By performing a force balance at the point where the actuated legs make contact with the ground, each of the phases can be characterized by an inequality constraint. For example, if  $F_{yG}(t)$  is selected as follows during the lifting phase

$$F_{yG} > \frac{m_L g}{\sin \phi} \quad (22)$$

<sup>3</sup>Hysteresis effects have been neglected for simplicity.

then the leg will lift and extend outward, where  $m_L \in R^1$  denotes a lumped mass that is supported by each leg and  $g \in R^1$  represents the gravity acceleration term. Since the right-hand side of (22) can be upper bounded by a known constant prior to the construction of the vehicle, it can be used to size the piezoelectric element and can be used as a constraint in the design of the linkage system. If  $F_{yG}(t)$  is selected as follows during the pulling phase

$$F_{yG} \leq \frac{m_L g \mu_s}{\cos \phi - \mu_s \sin \phi} \quad (23)$$

then the leg will rest on the surface and the vehicle will be pulled forward (note that rolling resistance and friction in the wheel have been neglected for simplicity), where  $\mu_s \in R^1$  represents the coefficient of static friction. If the inequality given in (23) is not satisfied during the pulling phase then the actuated leg will slip on the surface and no forward motion of the PMR will result. Based on the 13 constraint equations given in (8-16) and (18-21), the 13 unknown variables (i.e.,  $\theta_1(t)$ ,  $\theta_2(t)$ ,  $\theta_3(t)$ ,  $\theta_4(t)$ ,  $\theta_5(t)$ ,  $F_{yB}(t)$ ,  $F_{xC}(t)$ ,  $F_{yC}(t)$ ,  $F_{xD}(t)$ ,  $F_{yD}(t)$ ,  $F_{xE}(t)$ ,  $F_{yE}(t)$ , and  $F_{yG}(t)$ ) can be determined. Hence, given a desired position and orientation of the vehicle, the time derivative of the position of the actuated leg is determined by (4-7). Moreover, given the time derivative of the position of the actuated leg, (1) and (2) can be utilized to determine the joint angles. Given the joint angles, (12-15), (18) and (21) can then be utilized to determine the resulting forces.

*Remark 3:* Although the proposed flexure design avoids friction and wear, there is a possibility of joint fatigue due to the motion of the linkages. To avoid failure at a compliant joint, the thickness of the flexure sections was considered in the design process. The thicker the joint is made, the more stress the joint can withstand without failing; however, the motivation behind a compliant joint is to simulate a revolute joint, and hence, for increased flexibility that results in increased displacement amplification, the joint should be as thin as possible. By performing a mechanical optimization, a range of forces and joint displacements was determined at each joint. Based on this study, the thickness of the joints could then be designed to allow for maximum flexibility while maintaining a safety factor to eliminate joint failure. To calculate the deflection at the flexures, we utilized the following beam deflection equation

$$M = EI \frac{\partial y^2}{\partial x^2} \quad (24)$$

where  $M, I \in R^1$  represent a constant moment applied to the beam and the moment of inertia, respectively,  $E$  is given in (17), and  $x, y \in R^1$  represent the distance from the flexure point to the free end and the deflection of the beam, respectively (see Figure 6). After integrating (24) and utilizing the fact that

$$\theta_i = \frac{\partial y_i}{\partial x_i} \quad (25)$$

for the  $i$ -th joint, the following expression can be obtained

$$M_i = \frac{EI\theta_i}{L}. \quad (26)$$

Also, when a constant moment is applied to the joint, the normal stress acting on the  $i$ -th joint, denoted by  $\sigma_{ni} \in R^1$ , is given by the following expression

$$\sigma_{ni} = \frac{E\theta_i h_i}{2L}. \quad (27)$$

Moreover, the stress due to the tensile load at the  $i$ -th joint, denoted by  $\sigma_{ti} \in R^1$ , for a force  $F_i$  applied at the  $i$ -th joint,

is given by the following expression

$$\sigma_{ti} = \frac{F_i}{bh_i}. \quad (28)$$

Hence, the total stress at the  $i$ -th joint, denoted by  $\sigma_i \in R^1$ , can be determined as follows

$$\sigma_i = \frac{E\theta_i h_i}{2L} + \frac{F_i}{bh_i}. \quad (29)$$

*Remark 4:* Note that by dividing both sides of (26) by  $\theta_i$  and then utilizing the fact that

$$I = \frac{bh_i^3}{12} \quad (30)$$

for the linkages, the torsional spring constant for each joint given in (17) is obtained.

#### IV. MECHANICAL OPTIMIZATION

Given the number of constraints on the PMR and the various design choices (e.g., torsional stiffness of the joints, joint placement), an optimization procedure was performed to facilitate the design. Specifically, by constraining the footprint of the robot to be less than  $35 \times 10$  mm, the constraint equations given in (8-16), (18-21), and (29) were utilized to optimize the linkage length parameters to yield the maximum leg displacement. The maximum leg displacement was determined to be 107 times greater than the input displacement from the piezoelectric element. A fixed force of 0.2 N was applied to simulate a load on the leg during the optimization (this force was determined to be a conservative estimate based on the fact that the robot weight is less than 20 grams).

#### V. CLOSED-LOOP CONTROL

To develop a closed-loop controller to force the position and orientation of the PMR to track a desired trajectory (or follow a prespecified path), the position/orientation and linear/angular velocity of the PMR will be required. Since absolute position sensors like Global Position Sensors (GPS) or an overhead vision system are not viable options for many applications (although an overhead camera has been extensively utilized in many of the previous SEM applications), the passive wheel of the PMR is slotted (or notched) to provide odometry-based measurements of the aforementioned required signals. Given these measurements, a number of kinematic controllers can be designed (e.g., see [5]) based on (4) where the control input is expressed in terms of the linear and angular velocity of the PMR.

Although kinematic controllers that have been designed for traditional wheeled mobile vehicles can be utilized for the PMR, some special considerations must be made. For example, given the nature of the actuator design, restrictions must be placed on the reference trajectory. Specifically, since one actuated leg cannot produce a net negative velocity while the other leg produces a net positive velocity, the instantaneous center of rotation must lie on or outside the footprint of the legs (e.g., the robot cannot turn around a set point at the center of the robot as in traditional wheeled mobile vehicles). To enhance the robustness and performance of the control designs, the vehicle dynamics are typically incorporated into the overall control design; however, the dynamic model for the PMR will not exhibit the same characteristics as a traditional vehicle. For example, to achieve the maximum velocity of the PMR, the impedance of the compliant mechanical structure of the PMR will have to be adjusted based on the impedance of the piezoelectric element. Moreover, unlike traditional vehicles, the mass matrix will play a minor

role in the dynamic response of the vehicle when compared to the friction effects, and actuator disturbances must be incorporated to account for potential slip of the actuated leg (this is not modeled in the same manner as wheel slip for a standard mobile vehicle). In light of these control considerations, future work will target the development of a full dynamic model of the PMR and effort will be devoted to developing an outer-loop dynamic controller for a given inner-loop kinematic controller.

## VI. PROOF-OF-PRINCIPLE RESULTS

To illustrate that the proposed locomotion principle, including the ability of the compliant lever-based structure to amplify the piezoelectric forces, we developed and tested a prototype meso-scale robot (see Figure 7). To demonstrate the locomotion capabilities of the design, the following open-loop control voltage was applied

$$\frac{1}{2}(V_p \operatorname{sgn}(\cos(\omega t)) + V_p) \quad (31)$$

where  $V_p, \omega \in R^1$  represent the peak amplitude of the applied voltage and the radian frequency of the voltage, respectively, which were selected as follows

$$V_p = 100 \text{ volts}, \quad \omega = 3612 \text{ rad/sec.} \quad (32)$$

When the open-loop voltage given in (31) was applied, the PMR achieved speeds of 65 [cm/sec]. Based on the fact that the prototype robot illustrated in Figure 7 has only one actuator, the PMR was constrained to move in a straight line. Although the complete PMR design proposed in this paper has not been constructed, we believe that due to the results of the mechanical optimization, the use of a better wheel design, and the fact that the proposed PMR will have two piezoelectric elements actuating two legs the proposed PMR will be able to obtain speeds greater than 65 cm/sec.

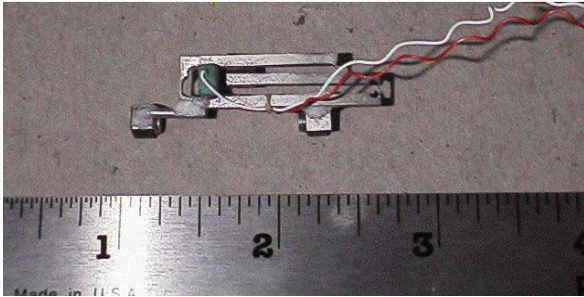


Fig. 7. Proof-of-principle PMR testbed

## VII. CONCLUSIONS

In this paper, a new piezo-based locomotion principle was applied to develop a meso-scale mobile robot. Specifically, inspired by [3], [4], and [9], the design utilizes a compliant lever-based flexural structure to amplify the displacement of a piezoelectric actuator by two orders of magnitude at the vehicle legs. The new locomotion principle contrasts with the slip/stick approach that is typically utilized for meso-scale mobile vehicles in that the assumption that the actuated legs slip on the surface is eliminated. A prototype PMR was constructed and utilized in a proof-of-principle demonstration. The results of these tests illustrated the feasibility of the new locomotion principle and indicated that significantly greater speeds could be obtained. Future efforts will target the development of a full dynamic model

for the vehicle, the development of an outer-loop dynamic controller, and the construction and testing of the complete vehicle.

**Acknowledgements:** We would like to thank Larry A. Pierce for fabricating the mobility platforms and for the helpful suggestions he made to the designs to make it a demonstrable robotic concept. We would also like to thank Dr. Steven L. Schrock for the assistance and support provided by the former Robotics and Process Systems Division at ORNL.

## REFERENCES

- [1] H. Aoyama and O. Fuchiwaki, "Flexible Micro-Processing by Multiple Micro Robots in SEM", *Proc. of the International Conference on Robotics and Automation*, pp. 3429-3434, 2001.
- [2] J.-M. Breguet, E. Pernette, and R. Clavel, "Stick and Slip Actuators and Parallel Architectures Dedicated to Microrobotics", *Proc. of the SPIE 2906*, pp. 13-24, 1996.
- [3] A. Cox, E. Garcia, and M. Goldfarb, "Actuator Development for a Flapping Microrobotic MAV", *SPIE Microrobotics Symp.*, pp. 102-108, Nov. 1998.
- [4] A. Cox, D. Monopoli, and M. Goldfarb, "Development of Piezoelectrically Actuated Elastodynamic Flapping Microaerial Devices", *ASME Adaptive Structures and Material Systems*, pp. 257-262, 1999.
- [5] W. E. Dixon, D. M. Dawson, E. Zergeroglu, and A. Behal, *Nonlinear Control of Wheeled Mobile Robots*, Vol. 262 Lecture Notes in Control and Information Sciences, Springer-Verlag London Ltd, 2000.
- [6] S. Fahlbusch, S. Fatikow, J. Seyfried, and A. Buerkle, "Flexible Microrobotic System MINIMAN: Design, Actuation Principle and Control", *Proc. of the IEEE/ASME International Conference on Advanced Intelligent Mechatronics*, pp. 156-161, 1999.
- [7] K. Ioi, "A mobile Micro-Robot Using Centrifugal Forces", *Proc. of the IEEE/ASME International Conference on Advanced Intelligent Mechatronics*, pp. 736-741, 1999.
- [8] K. Ioi, "Study on Turning Motion of Micro Robot Driven by Cyclic Force", *Proc. of the IEEE/ASME International Conference on Advanced Intelligent Mechatronics*, pp. 1319-1324, 2001.
- [9] S. Kota, J. Hetrick, Z. Li, and L. Saggere, "Tailoring Unconventional Actuators Using Compliant Transmissions: Design Methods and Applications", *IEEE/ASME Trans. on Mechatronics*, Vol. 4, No. 4, pp. 396-408, 1999.
- [10] G. Laurent and E. Piat, "Efficiency of Swimming Microrobots Using Ionic Polymer Metal Composite Actuators", *Proc. of the International Conference on Robotics and Automation*, pp. 3914-3919, 2001.
- [11] S. Martel, et al., "Three-Legged Wireless Miniature Robots for Mass-Scale Operations at the Sub-Atomic Scale", *Proc. of the International Conference on Robotics and Automation*, pp. 3423-3428, 2001.
- [12] S. Martel, A. Saraswat, and I. Hunter, "Fundamentals of Piezo-ceramic Actuation for Micrometer and Sub-micrometer Motions for the NanoWalker Robot", *Proc. of the SPIE, Microrobotics and Microassembly*, Vol. 4194, pp. 82-93, Nov. 2000.
- [13] S. Martel, A. Saraswat, A. Michel, and I. Hunter, "Preliminary Evaluation and Experimentation of the Push-slip Method for Achieving Micrometer and Sub-micrometer Step Sizes with a Miniature Piezo-actuated Three-legged Robot Operating Under High Normal Forces", *Proc. of the SPIE, Microrobotics and Microassembly*, Vol. 4194, pp. 141-148, Nov. 2000.
- [14] S. Martel, M. Szabelski, A. Leija, P. Madden, S. Lafontaine, and I. Hunter, "Initial Results of a New Type of Locomotion For a Wireless Instrumented Robot Capable of Subatomic Movements", *Proc. of the Biomedical Engineering Society and the 21st Annual International Conference of the IEEE Engineering in Medicine and Biology Society*, 1999.
- [15] F. Schmoedel and H. Wörn, "Remotely Controllable Mobile Microrobots Acting As Nano Positioners and Intelligent Tweezers in Scanning Electron Microscopes (SEMs)", *Proc. of the International Conference on Robotics and Automation*, pp. 3909-3913, 2001.
- [16] F. Schmoedel and S. Fatikow, "Smart Flexible Micro-robots for SEM Applications", *Journal of Intelligent and Robotic Systems*, in press.
- [17] M. Sitti, "PZT Actuated Four-Bar Mechanism with Two Flexible Links for Micromechanical Flying Insect Thorax", *Proc. of the International Conference on Robotics and Automation*, pp. 3893-3900, 2001.
- [18] T. Tanikawa and T. Arai, "Developing of a Micro-Manipulation System Having a Two-Fingered Mic-Hand", *IEEE Transactions on Robotics and Automation*, Vol 15, No. 1, pp. 152-162, Feb. 1999.
- [19] A. Teshigahara, M. Watanabe, N. Kawahara, Y. Ohtsuka, and T. Hattori, "Performance of a 7-mm Microfabricated Car", *IEEE/ASME Journal of Microelectromechanical Systems*, Vol. 4, No. 2, pp. 76-80, June 1995.
- [20] J. Yan, R. J. Wood, S. Avadhanula, M. Sitti, R. S. Fearing, "Towards Flapping Wing Control for a Micromechanical Flying Insect", *Proc. of the International Conference on Robotics and Automation*, pp. 3901-3908, 2001.
- [21] G. Yang, J. Gaines, and B. Nelson, "A Flexible Experimental Workcell for Efficient and Reliable Wafer-Level 3D Microassembly", *Proc. of the International Conference on Robotics and Automation*, pp. 133-138, 2001.